Direct Measurements of the Pressure Dependence of the Electron Temperature in a Magnetically Shielded Hall Thruster

IEPC-2024-821

Presented at the 38th International Electric Propulsion Conference, Toulouse, France
June 23-28, 2024

Madison G. Allen* and Parker J. Roberts† and Benjamin A. Jorns‡
University of Michigan, Ann Arbor, MI, 48109, USA

The electron temperature in the near-field plume of a 9-kW class Hall effect thruster is measured at five vacuum facility background pressures. Incoherent Thomson scattering is employed to measure the azimuthal electron velocity distribution along the center line of the Hall thruster channel. The electron temperature inferred from these distributions is then evaluated as a function of axial position at each pressure condition. Additionally, ion velocity measurements are acquired using laser-induced fluorescence to document changes in the acceleration of ions in a Hall thruster due to pressure. It is shown that the dependence of electron temperature on background pressure is correlated with that of the acceleration profile of the ion velocity. This relation is discussed in the context of possible explanations for the correlation including Ohmic heating and enhanced ionization in the channel.

I. Introduction

The influence of background pressure on the operation of Hall effect thrusters poses a major challenge for translating ground-based measurements to on-orbit performance. It is a well-known finding that ground Hall thruster behavior differs from flight behavior, and one of the key components driving this discrepancy is the varying background pressures between the two operating environments.[1–6] Due to limited pump capability, state of the art vacuum testing facilities cannot achieve comparable background pressures to the space environment. Given the importance of high fidelity ground testing, researchers have studied extensively the influence of the ground testing environment, termed as facility effects, by characterizing the pressure dependence on various performance metrics. It has been shown, for example, that increased pressure produces higher thrust, reduces the plume divergence, and alters plasma oscillations.[7,8] Various pressure studies also have demonstrated the pressure dependence of the acceleration region in a Hall thruster.[9–11] This region is characterized by where the electric field is maximized in the thruster channel and the ions experience the majority of their acceleration. It has been found that this region shifts upstream with increasing background pressure.

The physical processes that drive this movement of the acceleration zone with facility pressure are not well-understood. As a salient example, this effect has only been documented in the context of its impact on the ion dynamics. There remains an open question as to whether the spatial shift is correlated with other key aspects of the thruster's internal plasma properties. Most notably, given that the electric field is strongly coupled to the electron dynamics in the thruster channel, there is likely to be a strong correlation. In practice, however, how these electrons actually respond to pressure, and by extension the implications of this response for informing the driving mechanisms, have yet to be demonstrated. There thus is an apparent need

*PhD Candidate, Aerospace Engineering, mgallen@umich.edu
†PhD Candidate, Aerospace Engineering, pjrob@umich.edu
‡Associate Professor, Aerospace Engineering, bjorns@umich.edu

for a detailed, parametric investigation of the correlation between movement in electron and ion dynamics with facility pressure.

To this end, in this work, we employ a non-invasive diagnostic technique, incoherent Thomson scattering, to measure the azimuthal electron velocity distributions along the Hall thruster channel center line as a function of pressure. We similarly perform laser-induced fluorescence at various pressure conditions to generate ion velocity and electric field measurements for comparison.

This investigation is organized in the following way. In section II, we introduce the methodology behind the two diagnostics. In section III, we provide the experimental setup including the optics, thruster, and facility. In section IV, we provide the measurements from each diagnostic in this study. In section V, we discuss the relevant implications of the results. Finally, in section VI, we summarize this work and its key findings.

II. Methodology

In this section, we introduce the two diagnostics performed for this pressure study: incoherent Thomson scattering and laser-induced fluorescence. We discuss their background, key assumptions for their analysis, and the implementation for this test campaign to achieve both electron and ion velocity distributions at various pressure conditions.

A. Incoherent Thomson Scattering

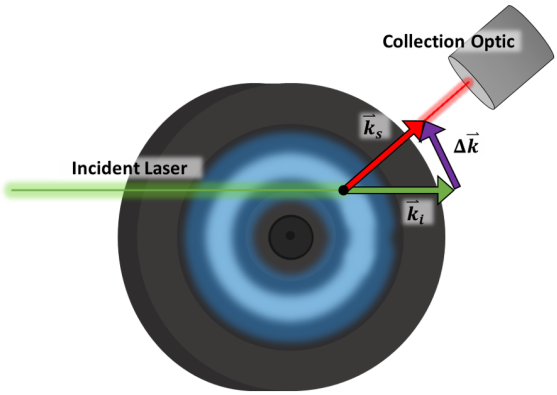

Figure 1: A diagram of the Incoherent Thomson scattering configuration for azimuthal electron motion measurements.

To measure electron velocity distributions, we utilize an incoherent Thomson scattering diagnostic. This plasma diagnostic has been implemented extensively when measuring electron properties for high-density plasma sources.[12,13] In recent work, it has been applied to low-density plasmas such as Hall effect thrusters.[14–17] For this diagnostic (Fig. 1), we measure the wavelength and intensity of photons at a given wavelength elastically scattered off of electrons. We invoke the Doppler shift where the scattered photon measures at a wavelength shift that corresponds with the velocity of that electron. For our experimental conditions, the Debye length of the plasma is far greater than the measured wavelength shift, thus the scattering process is described by the incoherent regime. This means that the phases of photons scattering from nearby electrons are uncorrelated, and thus coherent interference effects can be ignored. Subsequently, the intensity of the signal scales with the number of electrons scattered along the wave vector $\Delta\vec{k} = \vec{k}_s - \vec{k}_i$, where i is the incident light and s is the scattered light.

It can be shown that the the wavelength of the scattered length is Doppler shifted by the component of the velocity vector of the electrons in the direction of $\Delta\vec{k}$. As such, by strategically aligning the incident and scattered signals (Fig. 1), we can relate the velocity of electrons along this direction to the scattered wavelength:

$$v(\lambda) = c\frac{\left(\frac{\lambda_0}{\lambda} - 1\right)}{2\sin\frac{\theta}{2}}, \tag{1}$$

where v is the velocity projection in the direction of $\Delta\vec{k}$, c is the speed of light, λ_s is the observed wavelength, and λ_0 is the incident wavelength. The θ term represents the scattering angle between the incident and scattering vector.

In an ideal configuration, we can leverage the Doppler relationship to relate the incident of the scattered light at a given wavelength, $S(\lambda_s)$, to the density of electrons with velocity component parallel to $\Delta\vec{k}$, i.e. the electron velocity distribution function. This mapping can be expressed as $S(\lambda_s) \propto f(v)$ where the relationship between v and λ_s is given by Eq. 1. In a real configuration, the scattered signal is obscured by noise and stray light from the incident laser. It is therefore necessary to apply extensive amplification, filtering and background subtraction to extract the true signal. The details of this approach for our system are given in Ref. [18]

Following this signal isolation technique, the ITS ultimately yields a result for an intensity profile that is proportional to the projection of the velocity distribution function in the direction defined by $\Delta\vec{k}$. Fig. 2 shows an example result of a conditioned signal.

In order to extract information about the electron properties from this type of result, we assume in this work that the electron distribution function can be described by a Maxwellian distribution:

$$g(v) \propto \int A\sqrt{\frac{m_e}{2\pi k_B T_e}}\exp -\frac{m_e\left(v - u_d\right)^2}{2k_B T_e} I\left(v - v_I\right) dv_I. \tag{2}$$

Here f denotes the velocity distribution function, A is a constant, m_e is the electron mass, k_B is the Boltzmann constant, T_e is the electron temperature, u_d is a bulk or drift velocity, and I is an instrument broadening function.[18]

Figure 2 shows an example of the fit of Eq. 2 to experimental data where we treated A, T_e, u_d as free parameters. In this figure, the actual experimental data is at greater and smaller velocities than the region bounded by the dashed lines. This region, which is centered around the velocity of $v = 0$, corresponding to the wavelength of the incident light, is subject to enhanced filtering to prevent stray light from dominating the signal. This filtering alters the signal and is removed from the fitting procedure. The remaining fit thus yields data on temperature, density, and drift velocity.

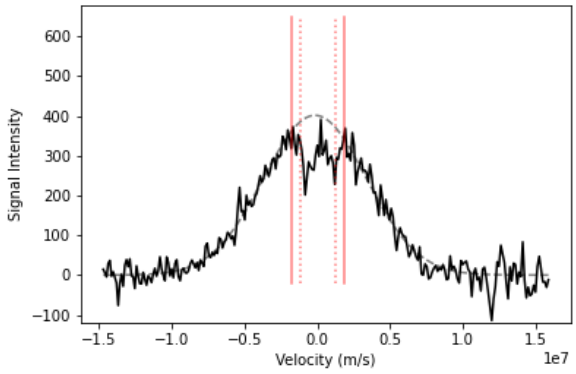

Figure 2: An example of the Maxwellian fit to ITS data with dashed bands for the laser light full width half max and solid bands for the masked data to incorporate broadening of the light

B. Laser-Induced Fluorescence

Laser-induced fluorescence is a diagnostic that measures ion velocity distributions for a fraction of ions in a small region of the plume. The mechanism behind this tool utilizes an incident laser light of a known wavelength to excite ions of a specific metastable energy state. The fluorescence emitted when the ion relaxes past the metastable state to a ground state is then collected and measured. The intensity of the signal is proportional to the density of ions while the wavelength of the laser introduced corresponds to a

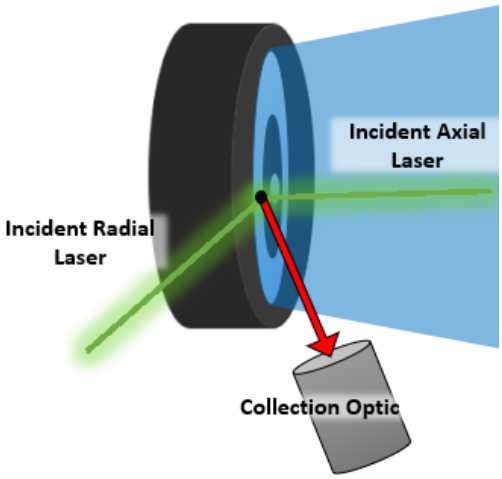

Figure 3: A diagram of the laser-induced fluorescence configuration for axial ion motion measurements.

given velocity. With that, similarly to Thomson scattering, laser-induced fluorescence employs the Doppler shift to measure ion velocity as a function of wavelength in the following format:

$$v\left(\lambda\right) = c\left(\frac{\lambda_0}{\lambda} - 1\right). \tag{3}$$

Unlike the Thomson scattering calculation, the collected light is not directional dependent. As the wavelength is varied, ions of each respective velocity are excited. Thus, we generate an ion velocity distribution (Fig. 4). This diagnostic is unique to each type of ion, including gas and charge state, but has become implemented across a variety of classes of Hall thrusters.[19,20]

Dissimilar to the electrons in the near-field of a Hall thruster, ions cannot be assumed to reach thermal equilibrium. Many results for ion velocity show a potential second population of ions captured with this diagnostic.[20] The approach has been to instead, fit a double Maxwellian distribution when a single does not encompass the full dataset. We provide the single and double Maxwellian distributions in the following equations,

$$g_1(v) = A_1\sqrt{\frac{m_i}{2\pi k_B T_i}}\exp\left(-\frac{m_i\left(v-u_d\right)^2}{2k_B T_i}\right), \tag{4}$$

$$g_2(v) = A_1\sqrt{\frac{m_i}{2\pi k_B T_{i,1}}}\exp\left(-\frac{m_i\left(v-u_{d,1}\right)^2}{2k_B T_{i,1}}\right) + A_2\sqrt{\frac{m_i}{2\pi k_B T_{i,2}}}\exp\left(-\frac{m_i\left(v-u_{d,2}\right)^2}{2k_B T_{i,2}}\right). \tag{5}$$

Here m_i denotes the ion mass, and the terms A, T_i, u_d represent fitting parameters for the scaling constant, ion temperature, and ion drift velocity, respectively.

In Figure 4, we demonstrate both the single and double Maxwellian fits for two different positions along channel center line. For each distribution, we determine the mean velocity using a weighted average. We also infer the electric field at each measurement location with the method established in Ref. [21]. This approach is based on considering a 1D Boltzmann equation for ions:

$$v_z\frac{\partial f}{\partial z} + a_z\frac{\partial f}{\partial v_z} = \nu f_0 \tag{6}$$

where v_z is ion velocity in the axial direction, z is axial position, f is the velocity distribution function, a_z is the axial acceleration, ν is the ionization frequency, and f_0 is the initial distribution function. This assumes steady state at each location and accounts for ionization. We solve for the acceleration in Eq. 6 by calculating various moments of the measured velocity distribution function. The electric field is then calculated with $E_z = m_i a_z/q$. With this understanding of the two diagnostics, we now move to the experimental setup.

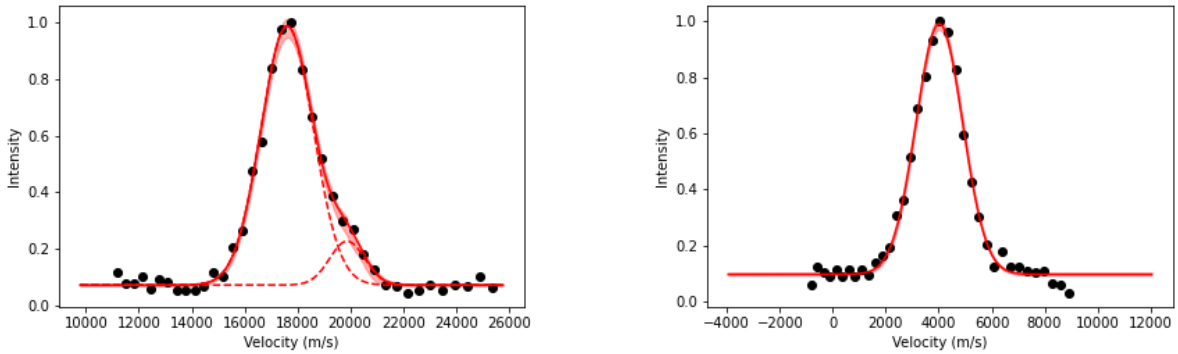

Figure 4: An example of the LIF IVDF traces and corresponding fits using a double Maxwellian (left) and a single Maxwellian (right).

III. Experimental Setup

A. Thruster and facility

We performed this experiment on the H9, a 9kW-class Hall effect thruster. This thruster was developed jointly with the University of Michigan, NASA Jet Propulsion Laboratory, and Air Force Research Laboratory. It is a magnetically shielded thruster with a boron-nitride discharge chamber and internally mounted cathode. The thruster rests on 3-axis motion stages to translate between alignment positions and measurement positions. We aligned the optics to measure at channel center line and move the thruster to measure different axial positions. The experiment was conducted in the Large Vacuum Test Facility at the University of Michigan with 14 cryopumps and a base operating pressure of 5 μTorr-Kr. The background pressure was measured using a Granville-Phillips® 370 Stabil-Ion® Vacuum Gauge with a neutralizer tube in the plane of the thruster and about 1 m off-axis. To vary the background pressure we inject neutral krypton gas with a 1/4" tube at the bottom of the chamber directed away from the exit plane. The tube was approximately 3 meters below the thruster. The pressure was controlled using 2 mass flow controllers rated to 800 sccm and 50 sccm allowing for fine adjustment.

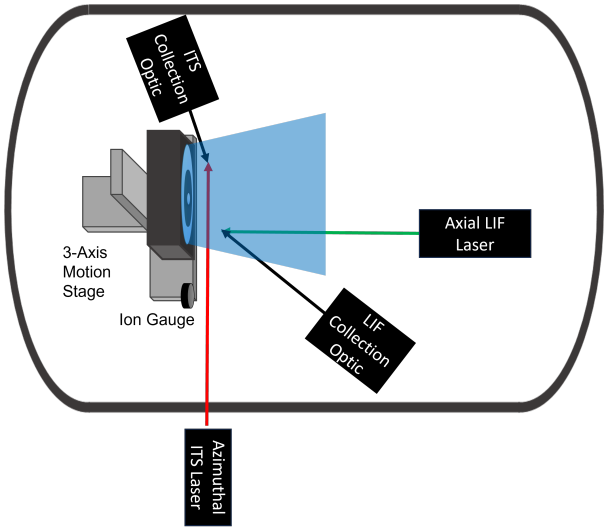

Figure 5: A diagram of the thruster and facility arrangement.

B. Operating conditions

For this test campaign, we operated the thruster at 4.5 kW and 300V on krypton with its nominal magnetic field strength. The discharge current was maintained across all pressure conditions by adjusting the total mass flow rate to the thruster. To achieve the various pressure conditions we backfilled neutral krypton at all of the higher pressure conditions. For higher pressure conditions, we used a different pumping configuration with fewer pumps. This is to offset the amount of backfilling required to achieve the higher background pressures. We provide the pressure conditions in Table 1. The change in anode flow is an indication of neutral ingestion. To maintain the same current less propellant is necessary due to supplemental background neutrals.

Background Pressure	5 μTorr	11μTorr	19μTorr	21μTorr	32μTorr
Number of Pumps	14	14	14	4	4
Anode Flow	13.40 mg/s	13.27 mg/s	13.00 mg/s	12.87 mg/s	12.73 mg/s

Table 1: The background pressure conditions

C. ITS optical bench

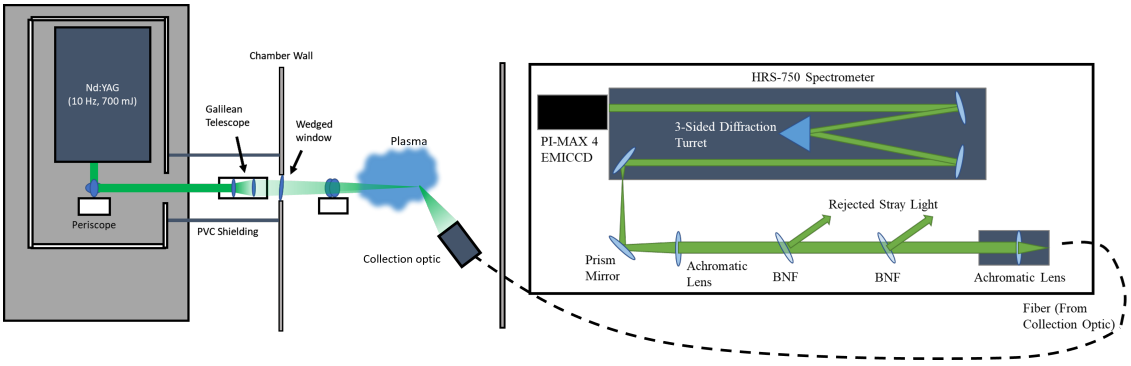

Figure 6: A diagram of the ITS optical setup

We show the Thomson scattering system in Fig. 6. It consisted of a Spectra Physics Quanta Ray Pro Q-switched Nd: YAG laser at 532 nm with the light positioned to enter the chamber through a wedged window and pass through periscope lenses to reach the near-field plume. We focused the laser and coinciding collection optic to measure along channel center line with the collection optic positioned at a 30° angle with respect to the incident light. This angle is the scattering angle seen in Eq. 1. The collected light passed through a fiber bundle to exit the chamber followed by three Bragg notch filters positioned to filter the returning laser light. The scattered signal is first processed through an HRS-750 Spectrometer and then measured by a Princeton Instruments MAX 4 EMICCD camera. For the electron velocity measurements, we captured 3000 images with the EMICCD camera to average over. We also acquired background shots to subtract light from the plasma itself and any electrical noise. We then fit the data with the Maxwellian distribution per our description in Sec. II A.

D. LIF optical bench

We display the laser-induced fluorescence setup in Fig. 7. We employed a Toptica Photonics tunable diode laser with a tapered amplifier for the laser radiation. We examined specifically the transition for KrII $5d^4D_{7/2} - 5p^4P^\circ_{5/2}$ which fluoresces at 729.98nm.[22,23] We passed the laser into a beam splitter for radial and axial components and through chopper motors at a frequency of 1.7 and 3.2 kHz. The injection laser entered the chamber through fiber optic bundles with the resulting fluorescence exiting the chamber similarly. A photomultiplier tube converted the signal to electron current, and a transimpedence amplifier transformed the current to voltage. We fed this voltage into a lock-in amplifier coupled to the chopper frequency which distinguished the axial and radial signal intensities and averaged the signal over a time constant of typically

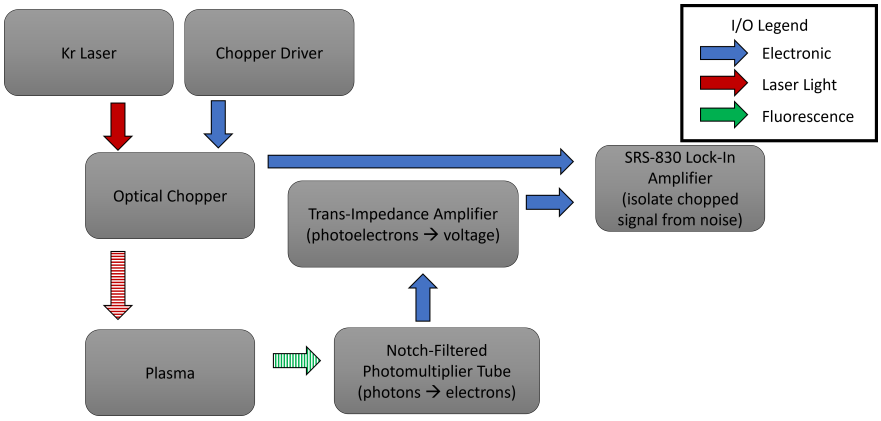

Figure 7: A diagram of the LIF optics table

300 ms. While we present the full optical configuration, we focus solely on the axial results. With this experimental setup, we will discuss the results of this experiment in the next section.

IV. Results

During the experiment, we operated the thruster until it reached thermal steady state, then performed the diagnostics. We monitored thruster and facility temperatures, as well as discharge oscillations. The thruster oscillations varied minimally between background pressure conditions. We show in Fig. 8 a summary of all the results from our study with the quantity of interest plotted on channel center line for different facility pressures. The first column shows the full extent of the measured domain while the right column shows a zoomed in view to highlight key features. We discuss each of these results in the following.

A. Ion Velocity Trends with Facility Pressure

We measured the axial ion velocity distributions at each pressure condition with laser induced fluorescence and then fit the data with a single or double Maxwellian distribution where applicable. We were able to measure a few points within the thruster channel and measure out to about 1 thruster channel length, L_{ch}. For each distribution, we calculated the mean velocity to clearly identify the region where ions experience the bulk of their acceleration. When comparing the results of different pressure conditions, we found a shift in the acceleration zone. This finding is consistent with previous laser-induced fluorescence studies.[9–11]

B. Electric field Trends with Facility Pressure

Following the method outlined in Sec. II A, we estimated the electric field along channel center line for multiple pressures. Figure 8 shows the resulting trends. As with the ion velocity data, there exists a similar upstream shift in electric field with increasing background pressure. With increased background pressure, the ion velocity profile illustrates that the applied electric force drives ions to their exhaust velocity closer to the thruster exit plane. Due to noise in the derivative calculation, the pressure trend is lost downstream of the peak field. Nevertheless, we are still able to resolve this peak in the electric field. We note that this apex translates to inside of the channel with increasing pressure. Now that we have demonstrated the pressure dependence for the electric field, we can compare this result to the measured electron temperature.

C. Electron Temperature Trends with Facility Pressure

Figure 8 shows our results for the electron temperature inferred from incoherent Thomson scattering as a function of position along channel center line for multiple background pressures. As can be seen, the temperature profile does appear to move upstream with increasing pressure. A notable result of this shift is that the peak in electron temperature, at $> 5\mu$Torr for this study, is no longer detectable in the measurement

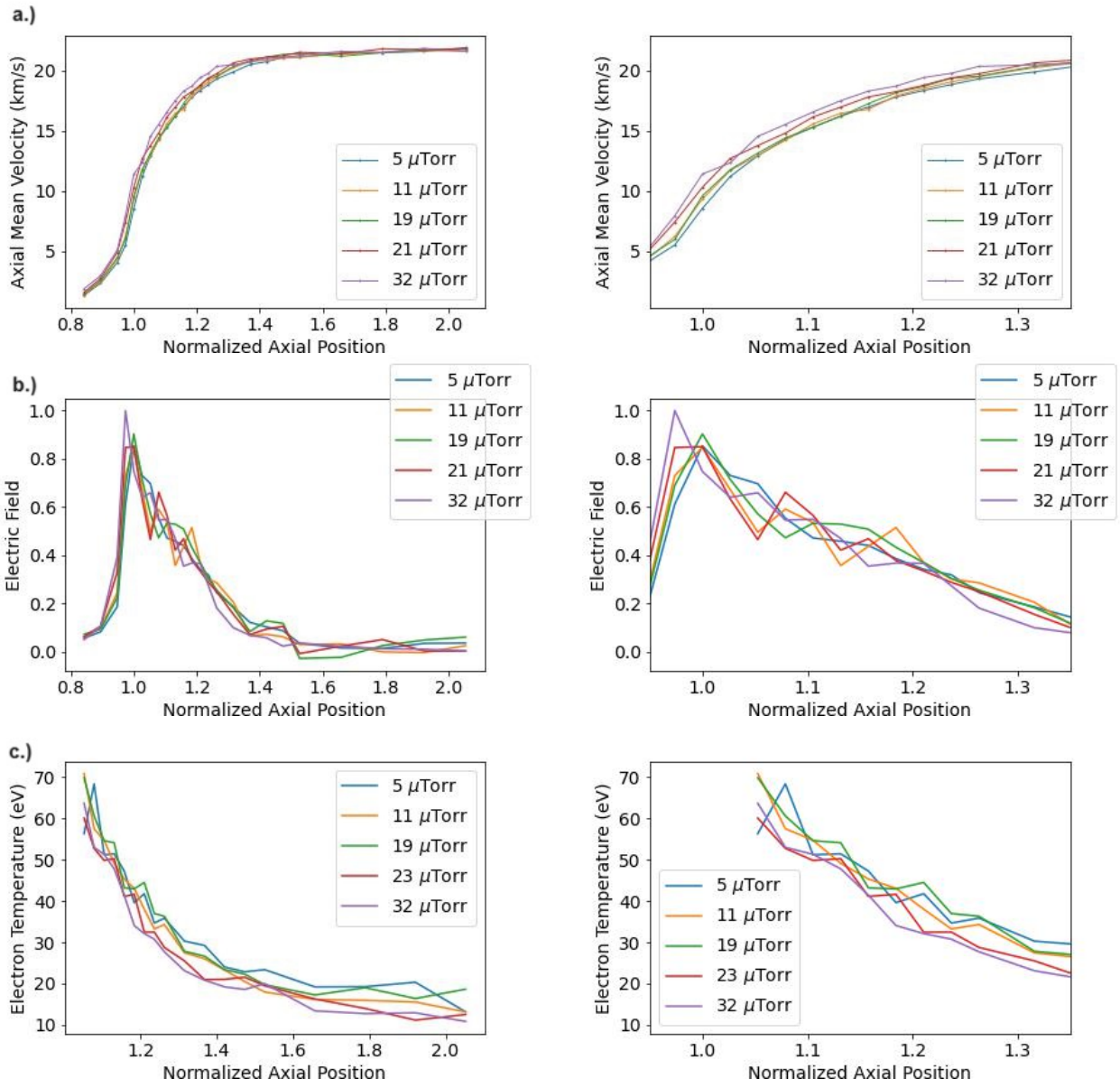

Figure 8: The mean ion velocity profile at the various pressure conditions (left) with a focus on the acceleration region with uncertainty shown (right). Electric field calculation at different pressure conditions along channel center line. The electron temperature trends at each background pressure condition.

domain of the diagnostic. This result thus confirms that the electron properties do in fact respond in a similar way to the ion dynamics.

D. Direct comparison of all datasets with pressure

As a final point of comparison, we show in Figure 9 contour plots of each quantity of interest as a function of pressure and axial position. A similar negative slope is apparent in each plot as further evidence of the overall profile shift across various parameters. We note, however, that the electron temperature profile does appear to shift to the same degree as the ion properties.

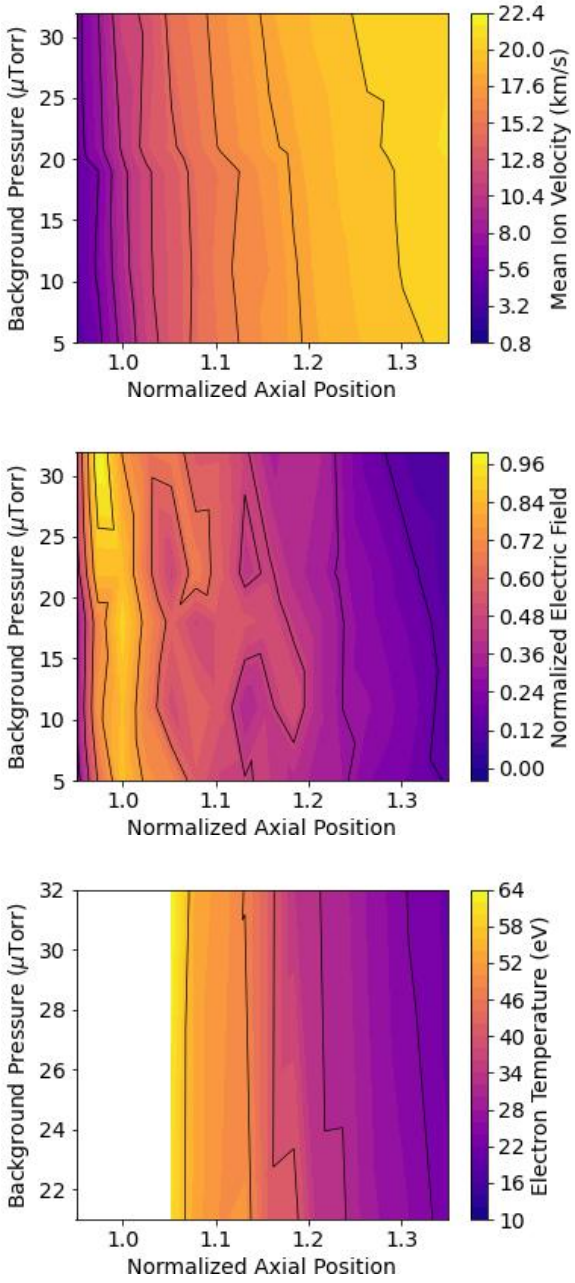

Figure 9: Contour plots of mean ion velocity, electric field, and electron temperature (left to right) as a function of pressure and axial position with black contour lines along constant values

V. Discussion

In this work, we have demonstrated a correlation between the changes in ion and electron properties with facility pressure. This result in turn invites the question as to what drives this relationship. We outline here two possible mechanisms.

The first we consider is that the shifts in electric field are causally driving the movement in electron temperature. This effect can be understood by considering that the electron temperature is a direct function of localized heating, which in turn scales with electric field magnitude. To 0th order, we might approximate $T_e \sim E^2$. In this case, we would anticipate the peak electric field to dictate the location of peak electron temperature, as shown in our results.

As an alternative, it is also possible that the shift in electric field (and thus ion trajectory) is driven causally by shifts in the electron temperature profile. To motivate, this we note from a generalized Ohm's law that the cross-field electron current, j_e, can be shown to be proportional to

$$j_e \propto E - \frac{\nabla(n_e T_e)}{n_e}, \tag{7}$$

where the two terms in the quantity represent electrostatic and pressure driven forces. Assuming, to first order, that the electron current is approximately constant in the channel, this relationship suggests that changes in electric field must be balanced by changes in the pressure driven force, i.e.

$$\delta E = \delta \frac{\nabla(n_e T_e)}{n_e}. \tag{8}$$

In this context, an upstream shift in the pressure term could result in an upstream shift in electric field, in order to maintain the same current. In this case then, the the pressure terms would drive the electric field response.

With that said, for both cases— electric field leading to pressure changes or pressure changes leading to electric field—the reason why these properties respond to pressure at all remains an open question. In the former scenario, if electric field movement is the driver, it may suggest that it is the response of electron mobility to pressure (related to the electric field through the Ohm's law) that is the key factor. In the latter case, the changes in pressure/temperature may be attributed to alterations in the energy balance that result from enhanced ionization from the background pressure. While the physical processes driving the pressure response ultimately remain outstanding, the fact that multiple key properties do move with pressure provides additional evidence for evaluating mechanisms that could explain these trends.

VI. Conclusion

In this work, we investigated the relationship of the pressure dependence between the ion and electron dynamics in the near-field Hall effect thruster plume. Specifically, we employed both laser-induced fluorescence and incoherent Thomson scattering to measure a sample of the ion and electron velocity distribution functions, respectively. We applied these tools to a magnetically shielded Hall thruster operating at five different background pressures. Using the method applied by Perez-Luna et al., we determined the electric field in the near-field plume at these various conditions, as well.[21] With these non-invasive techniques, we were able to observe a shift in the electron temperature trend that corresponded to the axial ion velocity and electric field effect. We have discussed how this relationship could be causal in both ways. On one hand, changes in temperature may be driven by the electric field. This could be explained by the fact that Ohmic heating is tied to the electric field, which in turn will influence the location of maximum temperature. We also have discussed the possibility that the change in temperature drive the shift in electric field. This could result, for example, if losses from enhanced ionization could be pushing the maximum electron temperature upstream. Through the Ohm's law, this could result in a shift in electric field upstream. It is also, of course, possible that both effects are convolved. With that said, regardless of the mechanism, our results have ultimately demonstrated that shifts in the plasma discharge driven by pressure are not isolated to the ion dynamics but rather influence the electrons too. This result ultimately may have direct implications for our understanding of this facility effect and the on-orbit operation of this system.

Acknowledgments

The authors would like to thank the NASA Space Technology Research Opportunity, Grant 80NSSC22K1172, as well as the NASA Research Institute, the Joint AdvaNced propUlsion inStitute (JANUS), for supporting this work. The first author would also like to thank Miron Liu for his experimental assistance.

References

[1] Randolph, T., Kim, V., Kaufman, H., Kozubsky, K., Zhurin, V., and Day, M., "Facility Effects on Stationary Plasma Thruster Testing," 1993.

[2] Sankovic, J. M., Hamley, J. A., and Haag, T. W., "Performance Evaluation of the Russian SPT-100 Thruster at NASA LeRC," 1993.

[3] Hofer, R. R., Peterson, P., and Gallimore, A., "Characterizing Vacuum Facility Backpressure Effects on the Performance of a Hall Thruster," *27th International Electric Propulsion Conference*, 2001, pp. IEPC–01–045. URL `http://adsabs.harvard.edu/abs/2005PhDT.....46W`.

[4] Byers, D., and Dankanich, J., "A Review of Facility Effects on Hall Effect Thrusters," 2009. URL `http://erps.spacegrant.org/uploads/images/images/iepc_articledownload_1988-2007/2009index/IEPC-2009-076.pdf`.

[5] Huang, W., Kamhawi, H., Haag, T. W., Ortega, A. L., and Mikellides, I. G., "Facility effect characterization test of NASA's HERMeS hall thruster," *52nd AIAA/SAE/ASEE Joint Propulsion Conference, 2016*, Vol. AIAA-2016-, 2016. https://doi.org/10.2514/6.2016-4828.

[6] Snyder, J. S., Lenguito, G., Frieman, J. D., Haag, T. W., and Mackey, J. A., "Effects of Background Pressure on SPT-140 Hall Thruster Performance," *Journal of Propulsion and Power*, Vol. 36, 2020, pp. 668–676. https://doi.org/10.2514/1.B37702.

[7] Diamant, K. D., Liang, R., and Corey, R. L., "The Effect of Background Pressure on SPT-100 Hall Thruster Performance," American Institute of Aeronautics and Astronautics, 2014. https://doi.org/10.2514/6.2014-3710.

[8] Huang, W., Kamhawi, H., Lobbia, R. B., and Brown, D. L., "Effect of background pressure on the plasma oscillation characteristics of the HiVHAc Hall thruster," *50th AIAA/ASME/SAE/ASEE Joint Propulsion Conference 2014*, 2014, pp. 1–14. https://doi.org/10.2514/6.2014-3708.

[9] MacDonald-Tenenbaum, N., Pratt, Q., Nakles, M., Pilgram, N., Holmes, M., and Hargus, W., "Background pressure effects on ion velocity distributions in an spt-100 hall thruster," *Journal of Propulsion and Power*, Vol. 35, 2019, pp. 403–412. https://doi.org/10.2514/1.B37133.

[10] Cusson, S. E., Dale, E. T., Jorns, B. A., and Gallimore, A. D., "Acceleration Region Dynamics in a Magnetically Shielded Hall Thruster," *Physics of Plasmas*, Vol. 26, 2019. https://doi.org/10.1063/1.5079414.

[11] Huang, W., and Kamhawi, H., "Facility Effects on the Ion Characteristics of a 12.5-Kilowatt Hall Thruster," *Journal of Propulsion and Power*, 2023, pp. 1–10. https://doi.org/10.2514/1.B39034.

[12] Carlstrom, T., Campbell, G., DeBoo, J., Evanko, R., Evans, J., Greenfield, C., Haskovec, J., Hsieh, C., McKee, E., Snider, R., et al., "Design and operation of the multipulse Thomson scattering diagnostic on DIII-D," *Review of scientific instruments*, Vol. 63, No. 10, 1992, pp. 4901–4906.

[13] Glenzer, S., Alley, W., Estabrook, K., De Groot, J., Haines, M., Hammer, J., Jadaud, J.-P., MacGowan, B., Moody, J., Rozmus, W., et al., "Thomson scattering from laser plasmas," *Physics of plasmas*, Vol. 6, No. 5, 1999, pp. 2117–2128.

[14] Vincent, B., Tsikata, S., Mazouffre, S., Minea, T., and Fils, J., "A compact new incoherent Thomson scattering diagnostic for low-temperature plasma studies," *Plasma Sources Science and Technology*, Vol. 27, 2018, p. 055002. https://doi.org/10.1088/1361-6595/aabd13.

[15] Vincent, B., Tsikata, S., and Mazouffre, S., "Incoherent Thomson scattering measurements of electron properties in a conventional and magnetically-shielded Hall thruster," *Plasma Sources Science and Technology*, Vol. 29, 2020, p. 035015. https://doi.org/10.1088/1361-6595/ab6c42.

[16] Roberts, P. J., and Jorns, B. A., "Laser Measurement of Anomalous Electron Diffusion in a Crossed-Field Plasma," *Physical Review Letters*, Vol. 132, 2024, p. 135301. https://doi.org/10.1103/PhysRevLett.132.135301.

[17] Roberts, P. J., and Jorns, B., "Inferring Electron Heat Flux in a High-Power Hall Thruster with Incoherent Thomson Scattering," American Institute of Aeronautics and Astronautics, 2024. https://doi.org/10.2514/6.2024-1957.

[18] Roberts, P., Allen, M., Brick, D., and Jorns, B., "Empirical Closure for Momentum and Energy Transport in Hall Thrusters Based on Thomson Scattering Measurements," 2024.

[19] Huang, W., Frieman, J. D., Kamhawi, H., Peterson, P. Y., Hofer, R. R., Branch, N. A., and Dao, H., "Ion Velocity Characterization of the 12.5-kW Advanced Electric Propulsion System Engineering Hall Thruster," American Institute of Aeronautics and Astronautics, 2021. https://doi.org/10.2514/6.2021-3432.

[20] Chaplin, V. H., Conversano, R. W., Lobbia, R. B., Ortega, A. L., Mikellides, I. G., Hofer, R. R., and Jorns, B. A., "Laser-Induced Fluorescence Measurements of the Acceleration Zone in the 12.5 kW HERMeS Hall Thruster," 2017.

[21] Pérez-Luna, J., Hagelaar, G. J. M., Garrigues, L., and Boeuf, J. P., "Method to obtain the electric field and the ionization frequency from laser induced fluorescence measurements," *Plasma Sources Science and Technology*, Vol. 18, 2009, p. 034008. https://doi.org/10.1088/0963-0252/18/3/034008.

[22] Hargus, W. A., Azarnia, G. M., and Nakles, M. R., "Kr II laser-induced fluorescence for measuring plasma acceleration," *Review of Scientific Instruments*, Vol. 83, 2012. https://doi.org/10.1063/1.4754889.

[23] Su, L. L., Marks, T. A., and Jorns, B. A., "Investigation into the Efficiency Gap between Krypton and Xenon Operation on a Magnetically Shielded Hall Thruster," 2022.